Nonlinear dynamics of mode-locking optical fiber ring lasers

Kristin M. Spaulding

Department of Applied Mathematics, University of Washington, Seattle, Washington 98195-2420

Darryl H. Yong

Applied and Computational Mathematics, California Institute of Technology, Pasadena, California 91125

Arnold D. Kim

Department of Mathematics, Stanford University, Stanford, California 94305-2125

J. Nathan Kutz

Department of Applied Mathematics, University of Washington, Seattle, Washington 98195-2420

Received April 20, 2001; revised manuscript received November 5, 2001

We consider a model of a mode-locked fiber ring laser for which the evolution of a propagating pulse in a birefringent optical fiber is periodically perturbed by rotation of the polarization state owing to the presence of a passive polarizer. The stable modes of operation of this laser that correspond to pulse trains with uniform amplitudes are fully classified. Four parameters, i.e., polarization, phase, amplitude, and chirp, are essential for an understanding of the resultant pulse-train uniformity. A reduced set of four coupled nonlinear differential equations that describe the leading-order pulse dynamics is found by use of the variational nature of the governing equations. Pulse-train uniformity is achieved in three parameter regimes in which the amplitude and the chirp decouple from the polarization and the phase. Alignment of the polarizer either near the slow or the fast axis of the fiber is sufficient to establish this stable mode locking. © 2002 Optical Society of America

OCIS codes: 140.0140, 140.3560, 140.3570, 060.5530, 060.4370, 060.0060.

1. INTRODUCTION

The nonlinear Schrödinger equation (NLS) governs the underlying wave behavior of an optical fiber that exhibits a weak Kerr nonlinearity.[1,2] The NLS has been investigated extensively in this context, with particular emphasis given to the robust and stable soliton solutions that result from a fundamental balance between linear dispersion and cubic nonlinearity. Thus soliton pulses are ideal carriers for transmitting optical data. For applications for which polarization effects are important, one must consider a system of coupled NLSs that is generally not integrable.[3] Despite the loss of integrability, solitonlike solutions are still found to persist.[4]

In addition to being ideal for long-haul communications applications,[5] solitons have also led to the development of the optical fiber ring laser.[6–9] For the ring laser configuration in Fig. 1 the Kerr nonlinearity of the birefringent optical fiber generates a nonlinear rotation of the polarization state that depends on the pulse intensity. The insertion of a passive polarizer then provides an effective intensity filter that stabilizes, or mode locks, a propagating pulse by periodically attenuating all components of the pulse that are not aligned with the polarizer. Simple devices such as these have been shown experimentally to generate stable and robust solitonlike pulse trains that can be used for a wide variety of telecommunications purposes.[6–10]

The two key modeling elements that describe the mode-locking dynamics are the inclusion of nonlinear polarization rotation induced by cross-phase modulation, and polarization control through the passive polarizer. In particular, we model optical pulses with coupled NLSs subject to periodic perturbations by the passive polarizer. This model allows us to examine the underlying mode-locking mechanism of the fiber ring lasers. As with previous studies,[11] our primary objective is to determine the performance characteristics of the laser, i.e., the uniformity of the resultant pulse train. To do so we utilize a reduced model for the pulse dynamics based on the robustness of soliton solutions and the variational character of the governing equations. In deriving this reduced model we neglect contributions from continuum radiation. One of the primary functions of the passive polarizer in the mode-locking process is to filter out this continuum radiation. Although a residual amount of radiation is expected from the periodicity of the cavity, it remains negligible in comparison with the energy in the localized mode-locked pulse. Hence we neglect radiation

0740-3224/2002/051045-10$15.00

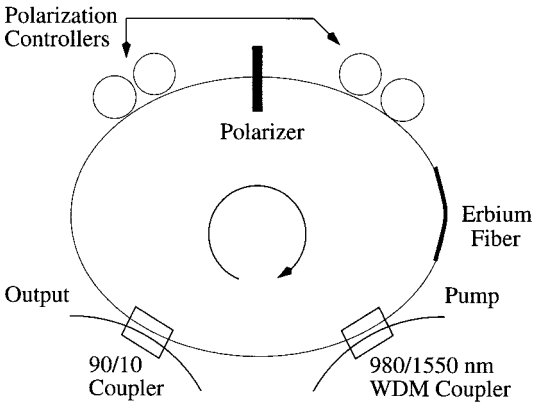

Fig. 1. Schematic of the ring cavity laser that includes a polarizer and polarization controllers in a birefringent optical fiber. A small portion of the fiber is erbium-doped fiber, which is pumped via a wavelength-division multiplexed (WDM) coupler at 980 nm and provides gain to the cavity. The mode-locked soliton pulse stream is coupled out through a 90/10 coupler; i.e., 10% of the pulse energy is coupled out. The two primary experimental parameters that can easily be adjusted are the polarizer angle relative to the fast and slow axes of the birefringent fiber and the birefringence strength, which is determined by the polarization controllers.

perturbations that emanate from the pulse reshaping process and from amplified spontaneous emission noise. This assumption leads to a reduction that isolates the fundamental interplay between the nonlinear polarization rotation and the polarization control element. This interplay and its resultant behavior are the focus of the present study.

In evaluating the uniformity of pulse trains generated by the laser we are interested primarily in reducing amplitude fluctuations. Quantities such as phase and polarization state are generally not relevant in experiments. Therefore we define stable mode locking here as the generation of a pulse train that has a nearly uniform amplitude. Although slight deviations from this uniform train are tolerated, the magnitude of the deviations is what determines the performance characteristics of the laser. Thus, for large amplitude fluctuations, the laser is operationally unstable, whereas small fluctuations lead to stable mode locking.

Amplitude fluctuations arise from a variety of physical effects, which include additive noise, physical instabilities in the cavity (i.e., mechanical or temperature), and fluctuations in the pump. However, we consider here the additional source of amplitude fluctuations that arises from the interplay between nonlinearity and polarization control. Our analysis describes the systematic and predictable amplitude fluctuations that result from this interaction. We note that these fluctuations are different from the chaotic instabilities generated in the laser as a result of nonlinearity.[12]

It was previously shown that alignment of the polarizer with the slow axis of the fiber results in a nearly perfect pulse stream.[11] However, that previous study considered only a small subset of possible solutions and focused on verifying the validity of the reduced model. Here we perform a more thorough investigation of the laser's modes of operation. Specifically, we have found analytically and numerically an additional region of operation for which the fiber laser generates a highly uniform pulse stream. In this paper we classify and explore the stability of each region of operation and show that the stable regions are phase locked, polarization locked, or both. This investigation represents what is to our knowledge the first comprehensive numerical and analytical study of the modes of operation of a fiber ring laser that is mode locked by a passive polarizer that accounts explicitly for the polarization dynamics.

The paper is organized as follows: In Section 2 we introduce a model for the mode-locking fiber laser. This model consists of the coupled NLSs with periodic perturbations that are due to the polarizer. In Section 3 we consider polarization-locked solutions that yield stable and uniform pulse trains when the polarizer is locked along the fast or the slow axis of the fiber. In Section 4 we continue by considering two possible phase-locked solutions that generate unstable pulse trains. In Section 5 we consider a final set of mode-locked solutions for which the polarization is assumed to remain fixed at the polarizer angle setting. The paper is concluded in Section 6 with a summary and highlights of significant results.

2. FORMULATION AND GOVERNING EQUATIONS

A. Pulse Propagation in Birefringent Fibers

The evolution of the slowly varying envelope of the electric field in an optical fiber subject to chromatic dispersion, Kerr nonlinearity, and polarization effects is given by the system of coupled nonlinear Schrödinger equations (CNLSs):

$$i\frac{\partial U}{\partial z} + \frac{1}{2}\frac{\partial^2 U}{\partial t^2} - KU + (|U|^2 + A|V|^2)U + BV^2U^* = 0, \tag{1a}$$

$$i\frac{\partial V}{\partial z} + \frac{1}{2}\frac{\partial^2 V}{\partial t^2} + KV + (A|U|^2 + |V|^2)V + BU^2V^* = 0. \tag{1b}$$

This system models linearly polarized light propagating in a birefringent optical fiber. Here we present Eqs. (1) in nondimensionalized form in which the U and V fields are orthogonally polarized components of the electric field. The birefringence strength parameter, K, determines the relative phase velocity difference between the U and V fields. The material properties of the optical fiber determine the values of nonlinear coupling parameters A and B. These parameters satisfy $A + B = 1$ by axisymmetry and, for the physical system considered here, take on the specific values $A = 2/3$ and $B = 1/3$. We have scaled complex orthogonal fields U and V on the peak field power $|E_0|^2$ that corresponds to the one-soliton solution of U when $V = 0$ and $K = 0$. The variable t represents the physical time normalized by $T_0/1.76$, where T_0 is the FWHM of a hyperbolic secant pulse and the variable z is the physical distance divided by dispersion length $Z_0 = (2\pi c)/(\lambda_0{}^2\bar{D}) \times (T_0/1.76)^2$. This gives a peak field power of $|E_0|^2 = (\lambda_0 A_{\text{eff}})/(2\pi n_2 Z_0)$. Here $n_2 = 2.6 \times 10^{-16}$ cm^2/W is the nonlinear index coefficient of the fiber, $A_{\text{eff}} = 55\ \mu$m^2 is the effective cross-sectional

area, $\bar{D}$ is the average cavity dispersion (in picoseconds per kilometer nanometer), $\lambda_0 = 1.55\ \mu$m is the free-space wavelength, and c is the speed of light.

We can recast the CNLS as a variational principle by defining its Lagrangian[13] and constructing an appropriate ansatz.[11] We assume, based on physical observations, that these pulses are approximately described by an amplitude and width fluctuation η, a polarization angle P, a relative phase ψ, a total phase ϕ, and a quadratic chirp β, which are related to the U and V fields as

$$U = \sqrt{I\eta}\,\mathrm{sech}(\eta t)\cos P \exp(-i\psi/2 + i\beta t^2 + i\phi/2), \tag{2a}$$

$$V = \sqrt{I\eta}\,\mathrm{sech}(\eta t)\sin P \exp(+i\psi/2 + i\beta t^2 + i\phi/2). \tag{2b}$$

Here we denote by I the initial energy contained within the pulse. In addition, we assume that these pulse parameters depend solely on z. Following Kim *et al.*,[11] we impose the condition that the variational derivatives of the Lagrangian with respect to P, ψ, η, and β be zero, and we obtain

$$\frac{dP}{dz} = {}^1\!/_3 BI\eta \sin(2P)\sin(2\psi), \tag{3a}$$

$$\frac{d\psi}{dz} = -{}^4\!/_3 BI\eta \cos(2P)\sin^2(\psi) + 2K, \tag{3b}$$

$$\frac{d\eta}{dz} = -2\beta\eta, \tag{3c}$$

$$\frac{\pi}{2}\frac{d\beta}{dz} = \eta^4 - \pi^2\beta^2 - I\eta^3[1 - B\sin^2(2P)\sin^2(\psi)]. \tag{3d}$$

This system of coupled ordinary differential equations (ODEs) models the leading-order pulse characteristics governed by the CNLS as long as the pulse remains close to the ansatz given in Eqs. (2). Extensive numerical simulations have been done to verify that the evolution of the pulse's characteristics governed by Eqs. (1) are well approximated by Eqs. (3).[11,13] This reduction from Eqs. (1)–(3) is a significant simplification of the mathematical model of the fiber laser, and we focus our attention on solutions of Eqs. (3). In this fiber cavity the variational analysis is expected to be in good agreement with the full model, provided that the loop length is of the order of the dispersion length or less. In this limit we also observed from full simulations that the continuum generation is negligible and thus can be neglected in the following analysis. Regardless, it is important to perform full numerical simulations to validate the assumptions in the ansatz.[11]

B. Periodic Passive Polarization Control

We model the optical fiber loop laser shown in Fig. 1 by using Eqs. (3) in a periodic domain that corresponds to loop length L. After a pulse propagates once around the fiber loop, it interacts with the polarizer. This polarizer attenuates the components of the pulse that are not aligned with polarizer angle Θ, resulting in a net rotation of the pulse's polarization state and a reduction of the pulse's amplitude, η. Afterward, erbium-doped fiber amplifiers boost the pulse's power back to the original cavity energy. Thus the polarizer–amplifier combination acts as a periodic perturbation on the pulse dynamics described by Eqs. (3). To simplify the modeling we consider this combination of polarizer and amplifier to be one operation that acts instantaneously after each round trip. This assumption is valid when the losses during each round trip are small.[11] Furthermore, we assume that the original input power is conserved throughout the laser such that this operation preserves power and is simply a rotation of the polarization state.

We define the polarizer angle, Θ, to be the angle between the alignment of the passive polarizer and the fast U axis. This convention is consistent with the definition of P and leads to the jump condition at the polarizer:

$$P_+ = \tan^{-1}[\alpha\tan(P_- - \Theta)] + \Theta, \tag{4}$$

where $P_\pm$ are the polarization angles before $(-)$ and after $(+)$ the polarizer. The polarizer strength parameter, α, indicates the efficiency of the polarizer in attenuating components not aligned with polarizer angle Θ. To be consistent with physical values, we consider $\alpha = 0.01$ such that the polarizer attenuates 99% of the pulse that is not aligned with the polarization angle.

The complete mode-locking model for the ring fiber laser thus consists of the system of CNLSs (3) and the polarization jump condition [Eq. (4)] that acts on the polarization angle after each round trip ($z = nL$ for $n = 1, 2, 3\ldots$). The two parameters of interest in this study are birefringence K and polarizer angle Θ.

A typical example of the mode-locking behavior is given in Fig. 2, which shows that arbitrarily chosen Gaussian-shaped initial conditions quickly settle to an amplitude-locked solution. For this computation, $\Theta = 0.45\pi$ and $K = 0.1$. The formation of these locked pulses is the focus of this study.

C. Stable Mode Locking through Pulse-Train Uniformity

The dynamics that result from the interaction between a pulse propagating in a birefringent fiber and the discrete action of the polarizer provide the foundation for understanding the mode-locking behavior. For operating these lasers the main concern is generating a train of pulses that have uniform amplitude and zero chirp. Thus we seek solutions of Eqs. (3) in which $\eta(z) = $ constant and $\beta(z) = 0$. This situation occurs when the amplitude and the chirp (η, β) dynamics decouple from the polarization and the phase (P, ψ) dynamics. From Eq. (3d) we see that this decoupling occurs when

$$C(P, \psi) = \sin^2[2P(z)]\sin^2[\psi(z)] = \text{constant}. \tag{5}$$

In this case the amplitude–chirp dynamics result in a simple phase-plane picture that has a center.[14,15] These center dynamics indicate that the laser can yield a uniform pulse train that gives rise to stable mode locking. So, although the phase and the polarization state are not relevant experimental quantities, these two parameters determine whether stable mode locking operation is possible.

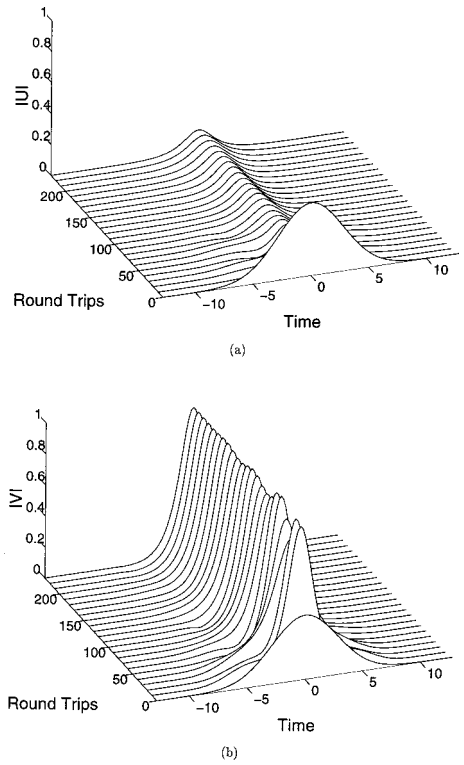

Fig. 2. Stable mode-locking evolution of the governing CNLSs with a polarizer. In this case we consider the parameters $\Theta = 0.45\pi$ and $K = 0.1$. Although the amplitude appears to lock to a constant value, a detailed look after each round trip of the cavity shows amplitude fluctuations on the order of 4% (see Fig. 7 below).

In as much as we can control the polarization state by aligning it with the passive polarizer ($P \approx \Theta$), Eq. (5) suggests that setting the polarizer angle to be $\Theta = 0$ or $\Theta = \pi/2$ results in $C(P, \psi) = 0$ because $\sin^2 2P \approx \sin^2 2\Theta = 0$. We show in the analysis that follows this section that these settings yield uniform pulse trains. Additionally, we can find a polarizer setting in which $\sin^2 2P \neq 0$ but for which the phase is constant and thus $\sin^2 2\psi =$ constant. This setting once again yields a stable mode-locked pulse stream whose phase and polarization state are both locked. We illustrate the importance of Eq. (5) to the operation of the mode-locked laser in the following sections. We note here that Eq. (5) further suggests that, if one is able to control the phase (i.e., if we can enforce $\psi \approx 0$ or $\psi \approx \pi/2$), then it is possible to generate mode-locked pulses by a phase-locking mechanism. By using phase-sensitive amplifiers[16–18] one may be able to incorporate an effective phase-locking mechanism to realize this situation.

3. POLARIZATION-LOCKED SOLUTIONS

In Subsection 2.C we showed that stable mode locking is possible when the polarization state is fixed at $P = 0$ or $P = \pi/2$ because in these cases $C(P, \psi)$ is a constant. In this section we examine these two situations in detail.

A. $P=0$

For $P = 0$, Eqs. (3) allow for a fixed point solution. The location of the fixed point and its stability can then be found by linearization, $P = P_0 + \tilde{P}$, $\psi = \psi_0 + \tilde{\psi}$, $\eta = \eta_0 + \tilde{\eta}$, and $\beta = \beta_0 + \tilde{\beta}$, where P_0, ψ_0, η_0, and β_0 are the leading-order solutions and $\tilde{P}$, $\tilde{\psi}$, $\tilde{\eta}$, and $\tilde{\beta}$ are small perturbations. At leading order it is clear from Eq. (3c) that we must take $\beta_0 = 0$ in order for $\eta_0 \neq 0$. Note that requiring $\eta_0 > 0$ arises from physical considerations of the pulse and the ansatz chosen in Eqs. (2). The remaining three equations require, to leading order, that

$$\sin 2P_0 \sin 2\psi_0 = 0, \tag{6a}$$

$$\cos 2P_0 \sin^2 \psi_0 = \frac{3K}{2BI\eta_0}, \tag{6b}$$

$$\eta_0 = I(1 - B \sin^2 2P_0 \sin^2 \psi_0). \tag{6c}$$

The last of Eqs. (6) determines the value of pulse amplitude η_0. Thus it only remains to determine the values of P_0 and ψ_0 that satisfy Eqs. (6a) and (6b).

The fixed point for $P_0 = 0$ is given by $P_0 = \beta_0 = 0$, $\eta_0 = I$, and $\psi_0 = \sin^{-1}(3K/2BI^2)^{1/2}$. Linearizing the 4×4 ODE system about this fixed point yields the four eigenvalues $\lambda = \{\pm 2iI^2/\pi, 2\gamma, -4\gamma\}$, where $\gamma = [K(2BI^2 - 3K)/3]^{1/2}$. The purely imaginary eigenvalues lead solely to oscillations, and the real eigenvalues (positive and negative) result in a saddle structure. We note that $2BI^2 - 3K > 0$ is automatically satisfied for the fixed point because $(3K/2BI^2)^{1/2} \leqslant 1$. For the typical values considered in this paper, $B = 1/3$ and $I = 1$, so $K < 2/9$. This restriction is consistent with physically realizable values of K, which generally tend to be one tenth or less for the fibers considered experimentally.

Although the underlying fiber evolution is unstable, the action of the polarizer stabilizes the dynamics by continually forcing the polarization state to be near $P = 0$. Provided that the polarizer acts on a sufficiently fast scale in comparison with the soliton evolution length, nearly uniform pulse trains can be realized. We illustrate this pulse propagation behavior in Fig. 3, where we demonstrate the evolution of the quantities of interest (η, β, P, and ψ) without a polarizer and with a polarizer. Here we have set $B = 1/3$ and $I = 1$. Note that, without a polarizer, the solution destabilizes and moves quickly away from the uniform amplitude- and polarization-locked solution. This destabilization is caused by the single growth mode near $P = 0$. In contrast, we note that the insertion of a polarizer forces the polarization state to remain near $P = 0$, so a nearly uniform pulse train can be generated and sustained for all time. Again, we point to the fact that $\Theta = 0$ forces $P \approx 0$ such that $C(P, \psi) \approx 0$ and an almost complete decoupling occurs between the amplitude–chirp dynamics and the phase and polarization evolution. This decoupling allows the amplitude–chirp dynamics to remain near the center. If the polarizer is detuned from $\Theta = 0$, large, quasi-periodic fluctuations result in the dynamics. This instability occurs despite the fact that the polarization state is locked on a value near $P = 0$. The degradation of the pulse trains uniformity is illustrated in Fig. 4 and shows the sensitivity of the mode locking to changes in the polarization state.

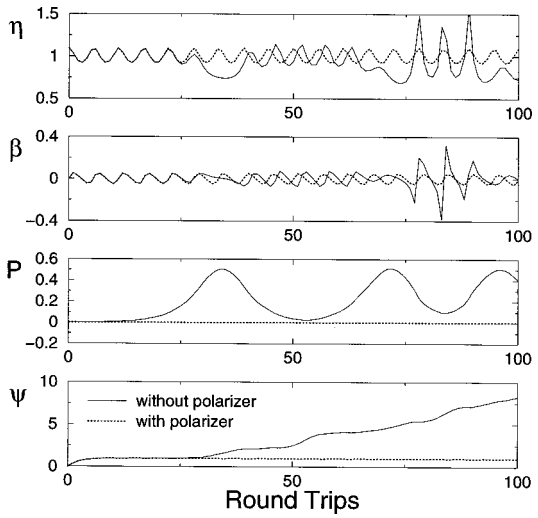

Fig. 3. Amplitude, chirp, polarization, and phase evolution over 100 round trips of the fiber cavity near the polarization-locked solution $P = 0$. $K = 0.10$, and the evolution without the polarizer has a single unstable eigenvalue leading to growth. This solution blows up just after $z = 150$. The addition of polarizer ensures that P remains near zero, so a uniform pulse train results.

B. $P = \pi/2$

Setting the passive polarizer to $\Theta = \pi/2$ also gives $C(P, \psi) = 0$. In contrast to the $P = 0$ case, no fixed point solution is found near $P = \pi/2$. However, this does not preclude the possibility of a stable mode-locked region. In particular, we find the z-dependent solution:

$$P(z) = \pi/2, \tag{7a}$$

$$\psi(z) = \tan^{-1}\left[\sqrt{\frac{3K}{\sigma}}\tan\left(\frac{2z\sqrt{3K\sigma}}{3}\right)\right], \tag{7b}$$

$$\eta(z) = I, \tag{7c}$$

$$\beta(z) = 0, \tag{7d}$$

which satisfies the system of ODEs (3) with $\psi(0) = 0$ and $\sigma = 3K + 2BI^2$. This solution has a phase that grows monotonically with distance z. Moreover, we have assumed without loss of generality that $\psi(0) = 0$ to simplify the expressions presented in Eqs. (7). However, the solution is locked at $P = \pi/2$, so a uniform pulse train is possible. It remains, however, to determine the stability of such a solution.

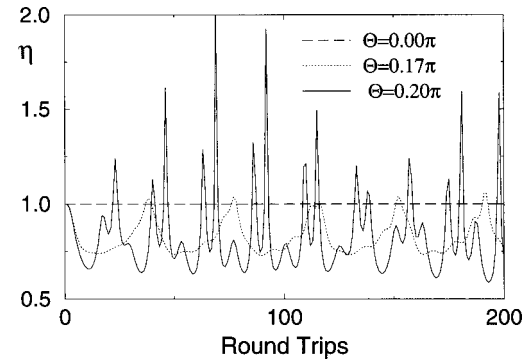

Fig. 4. Pulse-train uniformity (η fluctuations) over 200 round trips of the fiber cavity with $K = 0.10$ and near the polarization-locked solution $P = 0$. As the polarizer is detuned from $\Theta = 0$, the amplitude fluctuations increase and the pulse-train uniformity is destroyed.

We use a perturbation analysis to show that small perturbations about this known solution result in trajectories that remain close to it. In fact, the solution of Eqs. (7) has a centerlike behavior if we restrict our attention to the dynamics of P, η, and β. The perturbation analysis begins by expanding about the exact solution, $P(z) = P_0(z) + \epsilon P_1(z) + \ldots$, $\psi(z) = \psi_0(z) + \epsilon\psi_1(z) + \ldots$, $\eta(z) = \eta_0(z) + \epsilon\eta_1(z) + \ldots$, and $\beta(z) = \beta_0(z) + \epsilon\beta_1(z) + \ldots$, where the zero subscript indicates the leading-order solution given by Eqs. (7). We insert this solution into Eqs. (3) and solve the ODE that results at each order of ϵ, which is a small, positive parameter associated with the magnitude of the P perturbation. Using this perturbation expansion, we calculated a uniformly valid asymptotic solution to $O(\epsilon^2)$.

At $O(\epsilon)$, the perturbation analysis gives the almost periodic solution

$$\eta_1(z) = \eta_1(0)\cos\left(\frac{2I^2z}{\pi}\right) - \frac{\pi}{I}\beta_1(0)\sin\left(\frac{2I^2z}{\pi}\right), \tag{8a}$$

$$\beta_1(z) = \beta_1(0)\cos\left(\frac{2I^2z}{\pi}\right) + \frac{I}{\pi}\eta_1(0)\sin\left(\frac{2I^2z}{\pi}\right), \tag{8b}$$

$$P_1(z) = P_1(0)|\cos\Lambda z|\left(\frac{3K}{\sigma}\tan^2\Lambda z + 1\right)^{1/2}, \tag{8c}$$

$$\begin{aligned}\psi_1(z) = BK\pi\Bigg\{ & I\sin\left(\frac{2I^2z}{\pi}\right)[\eta_1(0)(4K\pi^2\sigma - 3I^4 \\ & + 3I^4\cos 2\Lambda z) + 2\pi^2 I\sqrt{K\sigma}\beta_1(0)\sin 2\Lambda z] \\ & + \pi\cos\left(\frac{2I^2z}{\pi}\right)[\beta_1(0)(4K\pi^2\sigma - 3I^4 \\ & + 3I^4\cos 2\Lambda z) - 2I^3\sqrt{K\sigma}\eta_1(0)\sin 2\Lambda z] \\ & - 4K\pi^3\sigma\beta_1(0)\Bigg\} \Big/ \big\{I^2(4K\pi^2\sigma - 3I^4) \\ & \times (\sigma - 2BI^2\sin^2\Lambda z)\big\},\end{aligned} \tag{8d}$$

where $\Lambda = \sqrt{4K\sigma/3}$ and we recall that $\sigma = 3K + 2BI^2$. Thus the perturbation analysis confirms that the solution, Eqs. (7), has a centerlike behavior. This implies that, even without a polarizer, pulses can be highly uniform. Inclusion of the polarizer further ensures that the polarization state of the pulse does not wander away from $\pi/2$, so this perturbation solution is valid. This analysis further shows that, under perturbation, or for polarizer angles near $\Theta = \pi/2$, the amplitude–chirp dynamics decouple from the polarization–phase dynamics. The resultant amplitude–chirp dynamics exhibits periodic fluctuations.[14,15] A comparison of the exact numerical solution to Eqs. (3) with the calculated perturbation is shown in Fig. 5. In this figure the polarization and the phase are calculated to the first correction, whereas the amplitude and the chirp are plotted with two correction terms. It can be seen that excellent agreement is

achieved with the exact numerical results. Extending the perturbation theory beyond the first correction is difficult because of the form of the phase and polarization terms. Thus only the first correction is considered for these two parameters. The full behavior of the solution with and without the polarizer is depicted in Fig. 6. We see that, even without the polarizer, the pulse train's uniformity is nearly preserved. The action of the polarizer further ensures that the pulse train is kept in control over all distances. The assumptions made in this model neglect perturbations that, for example, arise from additive noise, continuum generation, and pump fluctuations. The inclusion of such terms would destabilize the system in the absence of a polarizer. Within the context of the model, the results with and without the polarizer are essentially the same. Thus the fact that near $P = \pi/2$ the solution is stable allows for more-robust dynamics and stability. Figure 7 shows the resultant amplitude fluctuations as the polarizer is detuned from the ideal value of $\Theta = \pi/2$. Just as for detuning from $\Theta = 0$, the fluctuations grow and the laser is no longer thought of as operationally stable. This result is further addressed in Section 6 below.

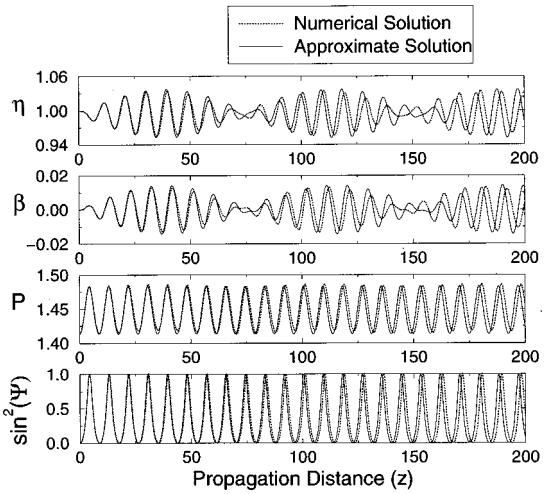

Fig. 5. Comparison of the exact numerical solution for $P \approx \pi/2$ with the perturbation expansion results for $\epsilon = 0.1$. Analytic data generated for phase (ψ) and polarization (P) include the leading-order solution and the first correction. The analytic curve of amplitude (η) and chirp (β) contains the leading-order solution and two correction terms. As the phase grows monotonically, it is more enlightening to examine $\sin^2\psi$ than ψ itself. Note that the perturbation results are in excellent agreement with the numerical results, except for a small phase slip observed in all quantities. In practice, this phase slip is unimportant, as we are concerned only with the size of the parameter fluctuations.

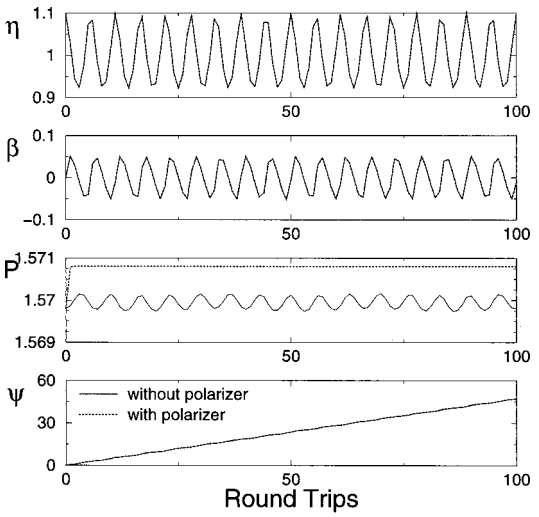

Fig. 6. Amplitude, chirp, polarization, and phase evolution over 100 round trips of the fiber cavity near the polarization-locked solution $P = \pi/2$. $K = 0.10$ and the evolution without the polarizer is a stable center. The addition of polarizer ensures that P remains near $\pi/2$, so the uniform pulse train is maintained.

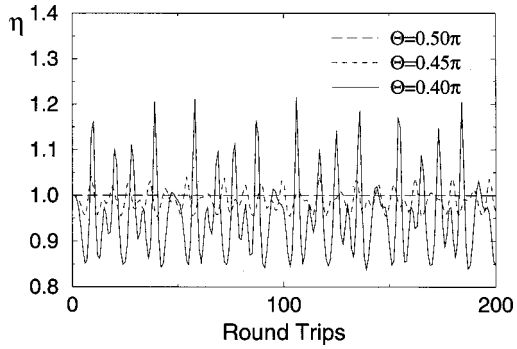

Fig. 7. Pulse-train uniformity (η fluctuations) over 200 round trips of the fiber cavity with $K = 0.10$ and near the polarization-locked solution $P = \pi/2$. As the polarizer is detuned from $\Theta = \pi/2$, the amplitude fluctuations increase and the pulse train's uniformity is destroyed. However, the uniformity here is not so severely affected as is detuning from $\Theta = 0$. (See Fig. 12 below).

4. PHASE-LOCKED SOLUTIONS

In addition to the polarization-locked solutions of Section 3, we can also consider phase-locked solutions and their associated stability. Of particular interest are the phase-locked solutions for which $\psi = 0, \pi/2$ because in these cases $C(P, \psi) = 0$, as in Section 3. These phase-locked solutions are easily found as fixed points of Eqs. (3). Note that Eqs. (6) give the conditions under which a fixed point can be found. Stability of these solutions can then be found by linearization.

A. $\psi_0 = 0$

When $\psi_0 = 0$, both Eqs. (6a) and (6b) are satisfied, provided that the birefringence is small, i.e., that $K = 0 + \tilde{K}$. This leaves the value of P_0 undetermined at leading order and gives $\eta_0 = I$ from Eq. (6c). We use these values to produce the linearized equations

$$\frac{d\tilde{P}}{dz} = 2/3BI^2 \sin 2P_0\tilde{\psi}, \tag{9a}$$

$$\frac{d\tilde{\psi}}{dz} = 0, \tag{9b}$$

$$\frac{d\tilde{\eta}}{dz} = -2I\tilde{\beta}, \tag{9c}$$

$$\frac{\pi^2}{2}\frac{d\tilde{\beta}}{dz} = I^3\tilde{\eta}. \tag{9d}$$

Equations (9c) and (9d) decouple from Eqs. (9a) and (9b), and the resultant dynamics for the amplitude and the chirp are oscillations given by

$$(\tilde{\eta},\tilde{\beta}) = \left[a_1\cos\left(\frac{2I^2}{\pi}z + a_2\right),\quad a_3\cos\left(\frac{2I^2}{\pi}z + a_4\right)\right], \tag{10}$$

where a_i are constants. Of greatest importance is the evolution of the polarization and phase states because they determine $C(P, \psi)$. From Eq. (9b) we find that $\tilde{\psi} = 2\tilde{K}z$, where it is assumed that $\tilde{\psi}(0) = 0$. This shows the phase to be unstable and further gives the following evolution of the polarization state:

$$\tilde{P} = [2/3B\tilde{K}I^2C\sin 2P_0]z^2, \tag{11}$$

which grows quadratically with distance z unless we choose $P_0 = 0$ or $P_0 = \pi/2$. Thus the $\psi_0 = 0$ phase-locked solution will be unstable owing to the growth of the phase and polarization states. Note that we already considered the $P = 0$ and $P = \pi/2$ states in Section 3.

B. $\psi_0 = \pi/2$

The case of $\psi_0 = \pi/2$ is drastically different from that of $\psi_0 = 0$ considered above. Here the leading-order solution for P_0 and η_0 with $\psi_0 = \pi/2$ is

$$\eta_0 = I(1 - B\sin^2 2P_0), \tag{12a}$$

$$\cos 2P_0 = \frac{3K}{2BI/\eta_0}. \tag{12b}$$

This solution leads to a cubic equation for leading-order amplitude η_0:

$$\eta_0{}^3 - I(1 - B)\eta_0{}^2 - \frac{9K^2}{4BI} = 0. \tag{13}$$

This cubic has three roots: one that is real and two that are complex conjugates. We consider only the real root because imaginary amplitudes are unphysical in Eqs. (2). We can then insert this value of η_0 into Eq. (12b) to determine the value of P_0.

The resultant linearized equations are given by

$$\frac{d\tilde{P}}{dz} = -{}^2/_3BI\eta_0\sin 2P_0\tilde{\psi}, \tag{14a}$$

$$\frac{d\tilde{\psi}}{dz} = -{}^4/_3BI(\cos 2P_0\tilde{\eta} - 2\eta_0\sin 2P_0\tilde{P}), \tag{14b}$$

$$\frac{d\tilde{\eta}}{dz} = -2\eta_0\tilde{\beta}, \tag{14c}$$

$$\frac{\pi^2}{2}\frac{d\beta}{dz} = \eta_0{}^3\tilde{\eta} + 2IB\eta_0{}^3\sin 4P_0\tilde{P}. \tag{14d}$$

Unlike in the previous case, the equations do not decouple. To determine stability, we evaluate the eigenvalues associated with the matrix on the right-hand side of Eq. (14). The resultant fourth-order polynomial for eigenvalue λ is given by

$$\lambda^2(\lambda^2 + 4\eta_0{}^4\pi^2) + \left(\frac{16}{81}\eta_0{}^2 - 4K^2\right) \times \left(\lambda^2 + \frac{4\eta_0{}^4}{\pi^2} + \frac{54}{\pi^2}\eta_0K^2\right) = 0, \tag{15}$$

where we have taken $I = 1$ and $B = 1/3$ for simplicity. If the real part of any of the eigenvalues λ is positive, instability occurs. The real parts of the eigenvalues are plotted in Fig. 8 and are shown to be strongly dependent on birefringence strength K. Beyond the critical value of $K = 2BI^2/3 \approx 2/9$, the fixed point ceases to exist.

Figure 8 predicts two regimes of stability. The first corresponds to values of birefringence of approximately $K \leqslant 0.14$, where there are two unstable and two stable eigenvalues. The linearized theory then predicts that the fixed point will be unstable. Figure 9 shows the slow growth of the solution away from the fixed point when one is starting close to $(P_0, \psi_0, \eta_0, \beta_0)$. It is reasonable to conjecture that the addition of the passive polarizer with $\Theta = P_0$ might stabilize the growth. However, Fig. 9 shows that the polarizer enhances the instability. This is so because the rotation that is due to the polarizer projects the solution further in the direction of the unstable eigenvectors, enhancing the growth.

The second physically realizable parameter regime of Fig. 8 corresponds to values of birefringence approximately $0.14 < K < 0.22$, where there are two pairs of purely imaginary eigenvalues. The linearized theory then predicts that the fixed point will be stable. Figure 10 shows the periodic behavior of solution near the fixed point when one is starting close to $(P_0, \psi_0, \eta_0, \beta_0)$. Unlike in the previous case in which $K = 0.10$, it would seem that the addition of the passive polarizer would maintain stability. However, once more numerical ex-

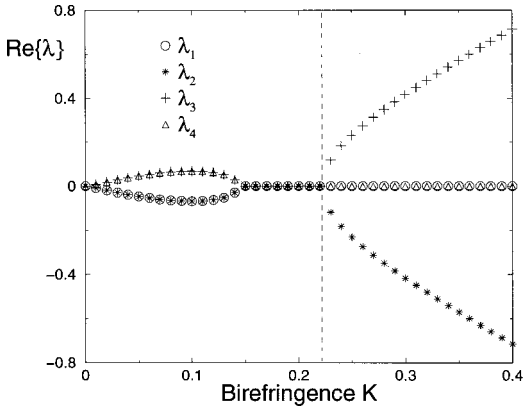

Fig. 8. Eigenvalues of the linearized equations for the phase-locked solution $\psi_0 = \pi/2$ as a function of birefringence K. Three distinct regions of operation are predicted; two of them are physically realizable. For $0 < K < 0.14$ there are two unstable and two stable eigenvalues, implying unstable growth. For $0.14 < K < 0.22$ the eigenvalues are all purely imaginary, and the solution is stable. The region to the right of the dashed line is not relevant physically, as it gives rise to imaginary values of P_0.

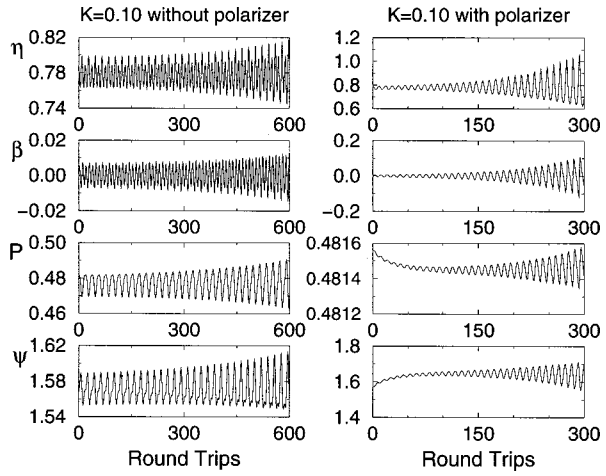

Fig. 9. Amplitude, chirp, polarization, and phase evolution over several hundred round trips of the fiber cavity near the phase-locked solution $\psi_0 = \pi/2$. $K = 0.10$, and the evolution without the polarizer has two unstable eigenvalues that lead to growth. The addition of the polarizer enhances the instability.

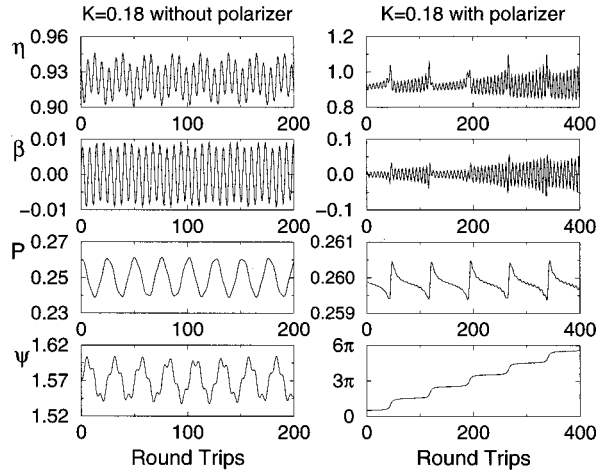

Fig. 10. Amplitude, chirp, polarization, and phase evolution over several hundred round trips of the fiber cavity near the phase-locked solution $\psi_0 = \pi/2$. $K = 0.18$, and the evolution without the polarizer has purely imaginary eigenvalues, leading to oscillations without growth. The addition of the polarizer destabilizes a uniform pulse train.

periments have shown otherwise, as demonstrated in Fig. 10. This instability is fundamentally different from that generated by Fig. 9 because there are no unstable eigenvalues. Note the 2π phase slip that is periodically generated from the action of the polarizer. We generate this slip by enforcing that the polarization stay fixed at $\Theta = P_0$.

5. OTHER REGIONS OF STABLE MODE LOCKING

Thus far we have considered the action of the polarizer as a separate and discrete action on the pulse evolution in the fiber. However, it is clear from Figs. 3, 4, 6, 7, 9, and 10 that the passive polarizer has the fundamental effect of preserving the polarization state of the propagating pulse. To model this effect we assume that the polarizer acts frequently enough that the polarization state effectively remains constant at the value set by the passive polarizer, i.e., $P = \Theta$. In this case the differential equation for P may be ignored. This assumption simplifies the analysis considerably because now the evolution equations reduce to a 3×3 system for the remaining parameters, η, β, and ψ. The resultant system has a fixed point:

$$\beta = 0, \tag{16a}$$

$$\eta = \frac{I}{2}\left\{1 + \left[1 - \frac{6K}{I}\sin(2\Theta)\tan(2\Theta)\right]^{1/2}\right\}, \tag{16b}$$

$$\psi = \pm\sin^{-1}\left[\frac{3K}{2BI\eta\cos(2\Theta)}\right]^{1/2}. \tag{16c}$$

In contrast to the previous solutions, the fixed point location is determined by the value of the birefringence, K. For this case the phase and polarization values force $C(P, \psi) \neq 0$.

The inclusion of a polarizer in this case quickly locks the amplitude, phase, polarization, and chirp parameters. Figure 11 demonstrates the uniform pulse train generated in this case. Note that the phase is also quickly locked to a constant value. The locked phase, chirp, and amplitude values are predicted in Eqs. (16) and are shown in Fig. 11 to be in excellent agreement with the numerical simulations. Here we have used the arbitrary values $K = 0.10$, $\eta(0) = 1.0$, $\psi(0) = \beta(0) = 0$, $P(0) = 0.0305\pi$, and $\Theta = 0.0305\pi$. The small resultant polarization fluctuations give an average value of $P \approx 0.0339\pi$. It is this value that we use to calculate the analytically predicted fixed point in Eqs. (16). This model provides yet another stable operating regime for the mode-locked laser because now both the phase and the polarization are locked and $C(P, \psi)$ is nearly constant.

This simplified model in which the polarization is assumed to remain constant ($P = \Theta$) predicts a whole family of solutions. In particular, this family of solutions includes the two fixed points associated with $P = 0$ and $\psi = \pi/2$. Furthermore, the value of Θ that produces $\psi = \pi/2$ is the maximum allowable polarizer angle that

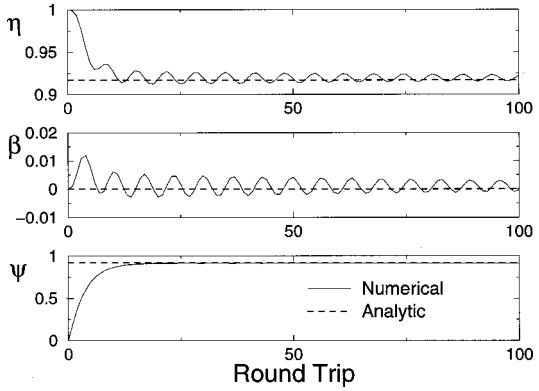

Fig. 11. Amplitude, chirp, and phase evolution over 100 round trips of the fiber cavity near the phase- and polarization-locked solution with $\Theta = 0.0305\pi$, $P(0) = 0.0305\pi$, $\eta(0) = 1.0$, $\psi(0) = \beta(0) = 0$, and $K = 0.10$. The addition of the polarizer stabilizes the otherwise unstable solution and quickly evolves to the predicted values of η, β, and ψ given by Eqs. (16).

generates real answers in Eqs. (16). Thus, although the solution near $P = \pi/2$ is inherently more stable, the stable mode-locking region near $P = 0$ has the possibility of being much bigger because of this fixed point branch of solutions for which $C(P, \psi) \approx$ constant.

6. CONCLUSION AND DISCUSSION

To summarize, we have considered the evolution of a pulse in a birefringent optical fiber with a periodic rotation of the polarization state that is due to a passive polarizer. Four parameters are essential for understanding the resultant pulse-train uniformity: polarization (P), phase (ψ), amplitude (η), and chirp (β). We found a reduced set of four coupled nonlinear differential equations that describe the leading-order pulse dynamics by utilizing the variational nature of the governing equations. Full numerical simulations of the governing equations validate the analytic model, provided that the cavity length is of the order of the dispersion length or less. Additive noise, continuum generation, and cavity instabilities can also be neglected in this limit. We found that, although the phase and the polarization are irrelevant to the experimentalist, these two parameters are essential for determining the pulse train's uniformity. In particular, the quantity $C(P, \psi) = \sin^2[2P(z)]\sin^2[\psi(z)]$ must remain nearly constant for pulse-train uniformity to occur and be maximized. Numerical simulations suggest that $C(P, \psi)$ must have less than $\approx$10% fluctuation to generate a stable mode-locked pulse train. Five possible operating regimes were found for the laser. Two of these regimes are unstable and correspond to phase-locked solutions where $C(P, \psi) = 0$ as a result of $\psi = 0, \pi/2$. The fact that these phase-locked solutions are unstable is not surprising because the polarizer can control only the polarization, not the phase. Two additional stable states were found for which $C(P, \psi) = 0$. These stable regimes correspond to $P = 0, \pi/2$. In contrast to the phase-locked solutions, these are easily stabilized by the laser because the polarizer acts to preserve the polarization state at these critical values. Thus uniform pulse trains can easily be generated. The remaining mode-locked solution arises from a simplified model in which the polarization state is assumed to be fixed at the polarizer angle ($P = \Theta$). This model gives a family of solutions that emanate from the polarization-locked $P = 0$ solution. This family of solutions was found to be stable.

The analysis provides valuable insight into the operation of the mode-locked laser. In particular, stable mode locking is defined by a nearly uniform pulse train. Our analysis addresses this issue directly and has found the key quantity, $C(P, \psi)$, which controls the mode-locking stability.

We finish this paper by providing one last figure, which illustrates the stable modes of operation of the ring laser. In this figure we evaluate the amplitude fluctuations for values of $\Theta \in [0, \pi/2]$. Here the vertical axis gives the passive polarizer angle Θ, and the horizontal axis gives the initial starting amplitude $\eta(0)$. The amplitude fluctuations are calculated for the last 50 of 100 round trips.

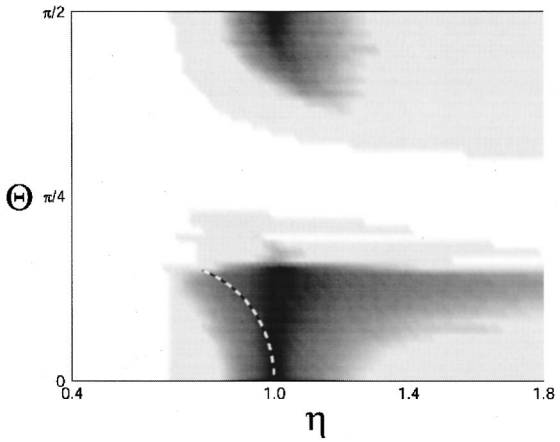

Fig. 12. Performance of fiber ring laser for $\Theta \in [0, \pi/2]$ with $K = 0.1$. Vertical axis, passive polarizer angle Θ; horizontal axis, initial starting amplitude $\eta(0)$. Near $\Theta = 0$ and $\Theta = \pi/2$ the laser produces uniform amplitude pulse solutions. Black, no pulse fluctuations; white, fluctuations greater than 20%. $B = 1/3$, $I = 1$, $\beta(0) = 0$, $L = 1$, and $\psi(0) = 0$. The fluctuation strength is calculated by consideration of minimum and maximum values of η fluctuations with its average value for values of η between round trips 50 and 100. Dashed curve, the family of solutions (16). Solutions away from $P = 0$ settle to this curve after many round trips until its termination at $\Theta \approx 0.1518\pi$. Average values of $\eta < 0.4$ are considered to be operationally unstable.

In particular, we compare the minimum and maximum amplitudes with their average to determine a percentage fluctuation. From a performance standpoint, we consider only pulse solutions that exhibit less than 20% fluctuation in power. Figure 12 shows a gray-scale plot of the regions of operation in which black corresponds to perfect mode locking (0% fluctuation) and white corresponds to unacceptable amplitude fluctuations (20% or greater fluctuation). For this figure the polarizer was set at the value of Θ indicated on the vertical axis, and the initial amplitude was varied from $0.4 < \eta < 1.8$. Near $\Theta = 0$ and $\Theta = \pi/2$ the evolution is stable, as predicted previously. Moreover, a large window of stable behavior exists near $P = 0$, which corresponds to solutions settling to the solutions given by Eqs. (16). The family of solutions (16) is depicted by the white dotted line in Fig. 12. This figure, which we believe is the first of its kind, serves as a guide to tuning the mode-locked fiber ring laser. Further, it suggests that mode locking near the fast and slow axes is crucial for achieving a uniform pulse train.

ACKNOWLEDGMENTS

We especially thank David Muraki for many valuable discussions pertaining to this research. Additionally, we thank the reviewers for their helpful comments, which have helped us to clarify several modeling issues in the paper. A. D. Kim and J. N. Kutz acknowledge support from the National Science Foundation (grants DMS-0071578 and DMS-0092682, respectively).

J. N. Kutz's e-mail address is kutz @amath.washington.edu.

REFERENCES

1. A. Hasegawa and F. Tappert, "Transmission of stationary nonlinear optical pulses in dispersive dielectric fibers," Appl. Phys. Lett. **23**, 142–170 (1973).
2. G. P. Agrawal, *Nonlinear Fiber Optics* (Academic, New York, 1989).
3. S. V. Manakov, "On the theory of two-dimensional stationary self-focusing of electro-magnetic waves," Sov. Phys. JETP **38**, 248–253 (1974).
4. S. Trillo, S. Wabnitz, E. M. Wright, and G. I. Stegeman, "Polarized soliton instability and branching in birefringent fibers," Opt. Commun. **70**, 166–172 (1989).
5. L. F. Mollenauer, P. V. Mamyshev, J. Gripp, M. J. Neubelt, N. Mamysheva, L. Grüner-Nielsen, and T. Veng, "Demonstration of massive wavelength-division multiplexing over transoceanic distances by use of dispersion-managed solitons," Opt. Lett. **25**, 704–706 (2000).
6. K. Tamura, H. A. Haus, and E. P. Ippen, "Self-starting additive pulse mode-locked erbium fiber ring laser," Electron. Lett. **28**, 2226–2227 (1992).
7. H. A. Haus, E. P. Ippen, and K. Tamura, "Additive-pulse modelocking in fiber lasers," IEEE J. Quantum Electron. **30**, 200–208 (1994).
8. M. Fermann, M. J. Andrejco, Y. Silverberg, and M. L. Stock, "Passive mode locking by using nonlinear polarization evolution in a polarizing-maintaining erbium-doped fiber laser," Opt. Lett. **18**, 894–896 (1993).
9. M. Hofer, M. E. Fermann, F. Haberl, M. H. Ober, and A. J. Schmidt, "Mode locking with cross-phase and self-phase modulation," Opt. Lett. **16**, 502–504 (1991).
10. B. C. Collings, S. T. Cundiff, N. N. Akhmediev, T. J. Soto-Crespo, K. Bergman, and W. H. Knox, "Polarization-locked temporal vector solitons in a fiber lasers: experiment," J. Opt. Soc. Am. B **17**, 354–365 (2000).
11. A. D. Kim, J. N. Kutz, and D. Muraki, "Pulse-train uniformity in optical fiber lasers passively mode-locked by nonlinear polarization rotation," IEEE J. Quantum Electron. **36**, 465–471 (2000).
12. G. Sucha, S. R. Bolton, S. Weiss, and D. S. Chemla, "Period doubling and quasi-periodicity in additive-pulse mode-locked lasers," Opt. Lett. **20**, 1794–1796 (1995).
13. D. J. Muraki and W. L. Kath, "Hamiltonian dynamics of solitons in optical fibers," Physica D **48**, 53–64 (1991).
14. J. N. Kutz, P. Holmes, S. G. Evangelides, and J. P. Gordon, "Hamiltonian dynamics of dispersion-managed breathers," J. Opt. Soc. Am. B **15**, 87–96 (1998).
15. P. Holmes and J. N. Kutz, "Dynamics and bifurcations of a planar map modelling dispersion managed breathers," SIAM J. Appl. Math. **59**, 1288–1302 (1999).
16. J. N. Kutz, C. Hile, W. L. Kath, R. D. Li, and P. Kumar, "Pulse propagation in nonlinear optical fiber lines that employ phase-sensitive parametric amplifiers," J. Opt. Soc. Am. B **11**, 2112–2123 (1994).
17. J. N. Kutz and W. L. Kath, "Stability of pulses in nonlinear optical fibers using phase-sensitive amplifiers," SIAM J. Appl. Math. **56**, 611–626 (1996).
18. A. D. Kim, C. G. Goedde, and W. L. Kath, "Stabilizing dark solitons by using periodic phase-sensitive amplifications," Opt. Lett. **21**, 465–467 (1996).